research articles Journal of proteome research

Modeling the Isoelectric Focusing of Peptides in an OFFGEL Multicompartment Cell

Hoang-Trang Lam, Jacques Josserand, Niels Lion, and H. H. Girault*

Laboratoire d'Electrochimie Physique et Analytique, Ecole Polytechnique Fédérale de Lausanne, Station 6, CH-1015 Lausanne, Switzerland

Received November 15, 2006

In proteomic analysis of complex samples at the peptide level (termed shotgun proteomics), an effective prefractionation is crucial to decrease the complexity of the peptide mixture for further analysis. In this perspective, the high-resolving power of the IEF fractionation step is a determining parameter, in order to obtain well-defined fractions and correct information on peptide isoelectric points, to provide an additional filter for protein identification. Here, we explore the resolving power of OFFGEL IEF as a prefractionation tool to separate peptides. By modeling the peak width evolution versus the peptide charge gradient at p*I*, we demonstrate that for the three proteomes considered *in silico* (*Deinococcus radiodurans*, *Saccharomyces cerevisiae*, and *Homo sapiens*), 90% of the peptides should be correctly focused and recovered in two wells at most. This result strongly suggests OFFGEL to be used as a powerful fractionation tool in shotgun proteomics. The influence of the height and shape of the compartments is also investigated, to give the optimal cell dimensions for an enhanced peptide recovery and fast focusing time.

Keywords: isoelectric focusing • isoelectric point • OFFGEL electrophoresis • IPG • shotgun proteomics • peptide fractionation • finite element model • numerical simulation

1. Introduction

Isoelectric focusing (IEF) is a high-resolution electrophoretic technique used to separate and concentrate amphoteric biomolecules at their isoelectric point (p*I*) in a pH gradient and under the application of an electric field. IEF is classically used in buffered free solution (in the presence of so-called carrier ampholytes), or in Immobilized pH Gradient (IPG) gels. In the past decades, isoelectric focusing has gained great significance due to its wide applicability in different fields.

In the field of proteomics, in-gel IEF of proteins is used routinely as the first dimension of two-dimensional gel electrophoresis,[1,2] which remains the workhorse for proteome analysis.[3] But because further protein analysis and characterization by mass spectrometry[4] require tedious sample preparation, new IEF schemes and devices have been designed for prefractionation of proteins by IEF:[5,6] several teams have explored the use of free-flow electrophoresis for the fractionation of proteomic samples.[7−12] Righetti et al. have introduced multicompartment electrolyzers, in which proteins are separated into different compartments separated by Immobiline membranes.[13−15] Wall et al. have also validated the use of Rotofor for fractionation of proteins prior to RP−HPLC and MALDI-TOF analysis of intact proteins.[16] We have introduced a new concept named OFFGEL IEF with the first aim to purify proteins.[17] The technique was later successfully used for the isoelectric fractionation of *Escherichia coli* proteins, proving to be a promising tool for proteomic applications.[18]

Besides these general efforts to develop IEF for protein fractionation, IEF has also been used for peptide separation in a shotgun approach, where proteins are first proteolized, and the resulting peptides mixture separated and analyzed by tandem mass spectrometry. Several groups have used in-gel IEF as a first separation dimension in shotgun proteomics,[19−23] as well as free-flow electrophoresis[24−26] and homemade devices based on Immobiline membranes.[27−29] OFFGEL IEF was demonstrated to be of great interest in shotgun proteomics;[30−34] a commercial device is now marketed by Agilent Technologies. But not only does IEF provide a separation means for peptides, but it also provides an additional physicochemical information about each peptide, its isoelectric point, which can then be used to validate MS/MS peptide sequence identification, and ultimately filter out false peptide identifications.[20−23,30−32] IEF separation of peptides can thus play a crucial role, not only as an efficient separation dimension, but also as a validation/filtering tool when combined with tandem mass spectrometry. As such, it is thus relevant to optimize devices used to separate peptides by IEF, such as OFFGEL.

The multiwell format of OFFGEL electrophoresis initially consists in placing the sample in wells, which are opened at top and bottom extremities and are placed on an IPG gel. The gel buffers a thin layer of the solution in the liquid chambers, and the proteins are charged according to their p*I* and to the pH imposed by the underlying gel. Two electrodes are respectively placed in the extreme compartments of the setup (lowest

* To whom the correspondence should be addressed. E-mail: hubert.girault@epfl.ch.

10.1021/pr0606023 CCC: $37.00
Published on Web 03/31/2007

and highest pH). Upon application of an electric field, the charged species migrate through the gel from well to well until they reach the well where they are neutral (pI = pH gel) and from where they are directly recovered in solution. For the solution to be buffered by the Immobilines present in the gel, the ampholyte concentration in the solution must not be too high and the buffering capacity of the gel must be efficient. Numerical simulations were used to study the influence of the ampholyte concentration in solution and the buffering capacity in OFFGEL IEF.[35]

Dynamic computer simulation of electrophoresis has already demonstrated considerable value as a research tool. Since the 1980s, numerical simulations have been performed to better understand and describe IEF[36−40] and have shown a qualitative agreement between predictions and experimental results. Recent advances in computer simulation have led to the development of a simulator that can handle up to 150 components and voltages typically used in experiments. This recently allowed Thormann et al. to perform the simulation of the dynamics of protein IEF in the presence of a large number of carrier ampholytes.[41,42] Computer simulation of immobilized pH gradient gels were also done, at acidic and alkaline conditions, showing the focusing dynamics, as well as the conductivity and buffering capacity in these regions.[43] Previous works had already led to the creation of a pH gradient simulator for the engineering of IPG gels and isoelectric membranes.[44,45] Regarding OFFGEL electrophoresis, the buffering capacity has been studied numerically, and a model has also been developed to describe the isoelectric separation of two simple ampholytes in a 2-D chamber.[46]

In this paper, we have addressed the questions how sharp the separation of peptides by OFFGEL IEF is and how the fractionation cell can be optimized to obtain the best resolution in the shortest time. We have taken as model biomolecules the peptides generated by *in silico* digestion of the proteomes of *Deinococcus radiodurans*, *Saccharomyces cerevisiae*, and *Homo sapiens* and simulated the OFFGEL isoelectric focusing in a multicompartment device. The peptide charge slope at pI was demonstrated to be a key parameter in the focusing dynamics, and its influence on the peak width and focusing time was studied in order to determine the proportion of correctly focused peptides (peptides recovered in one or two wells at most). This allowed the determination of the optimal well width to obtain the best focusing. The effects of the well height and shape were further studied, to determine the well configuration allowing the highest peptide recovery in the shortest time. In this analysis, we show that the high-resolving power of OFFGEL makes it a highly valuable tool to fractionate peptides in shotgun proteomics, and that it is relevant to optimize the fractionation unit to obtain the best recovery.

2. Methods

2.1. Analytical Model. The isoelectric point (pI) of a peptide is the pH at which the sum of all the electrical charges is equal to zero. In a peptide, the global charge can be calculated by taking into account the charge of the N-terminus (N-ter) and the C-terminus (C-ter), as well as the charge of ionizable side chains. In addition to the N-terminus, the positive charges can be provided by three amino acids which are lysine (K), arginine (R), and histidine (H). The negative charges originate from the C-terminus and four amino acids, tyrosine (Y), cysteine (C), aspartate (D), and glutamate (E). The charges of the ionizable groups depend on their pK_a values and on the local value of the pH. For a given ionizable amino acid i, the positive charge z_i^+ (pH) or the negative charge z_i^- (pH) is estimated from Henderson−Hasselbach's equation

$$z_i^+(\mathrm{pH}) = \frac{1}{1 + \frac{K_i}{10^{-\mathrm{pH}}}} \tag{1}$$

$$z_i^-(\mathrm{pH}) = -\frac{1}{1 + \frac{10^{-\mathrm{pH}}}{K_i}} \tag{2}$$

where K_i is the acidic dissociation constant of the amino acid i.

Under these assumptions, the global charge of a peptide can be expressed as follows:

$$z(\mathrm{pH}) = -\sum_{i\in A^-} \frac{1}{1 + \frac{10^{-\mathrm{pH}}}{K_i}} + \sum_{i\in A^+} \frac{1}{1 + \frac{K_i}{10^{-\mathrm{pH}}}} \tag{3}$$

where $A^- = \{\mathrm{Y, C, D, E, C\text{-}ter}\}$ and $A^+ = \{\mathrm{K, R, H, N\text{-}ter}\}$.

This approach assumes that the pK_a value of an ionizable group is independent of its position in the molecule, and that all the individual acid−base equilibria can be considered as independent. It should be noted that the calculated pI depends considerably on the set of pK values assumed for the ionizable groups. It was shown that when different sets of published pK values were used; the predicted pI of some proteins or peptides differed by up to 1 pH unit.[47] However, the aim of the present paper is to describe the focusing phenomenon in an OFFGEL device, rather than to give exact values of pI. All the data presented in this study use the pK values of amino acids from ref 48 (Supporting Information 1). Other values from Expasy[49] and Promost[50] have been used and qualitatively showed the same distributions for peptide pI and charge derivative (results not shown).

For a stationary regime of isoelectric focusing without chemical reactions, the equation of conservation of flux is given by

$$\frac{\partial c_i}{\partial t} = -\mathrm{div} J_i = 0 \tag{4}$$

where c_i and J_i are the concentration and the flux density of species i. Considering only the diffusion−migration transport in one direction, this equation reduces to the following 1-D steady-state equation:

$$\frac{\partial}{\partial x}\left(-D_i\frac{\partial c_i}{\partial x} - \frac{z_i F}{RT} D_i c_i \frac{\partial \phi}{\partial x}\right) = 0 \tag{5}$$

where D_i and z_i are the diffusion coefficient of species i and its charge as calculated in eq 3. F is the Faraday constant, R is the molar gas constant, T is the temperature, and ϕ is the local electric potential.

It results from eq 5 that the flux of species i (term in brackets) is uniform over x. Since at the isoelectric point, the concentration is maximal and the charge zero, the global flux at the steady-state is zero. The flux of species due to diffusion is thus compensated by the flux due to electromigration, leading to eq 6.

$$\frac{\partial c_i}{\partial x} = \frac{FE}{RT} z_i(x) c_i(x) \quad (\text{where } E = -\nabla\phi) \tag{6}$$

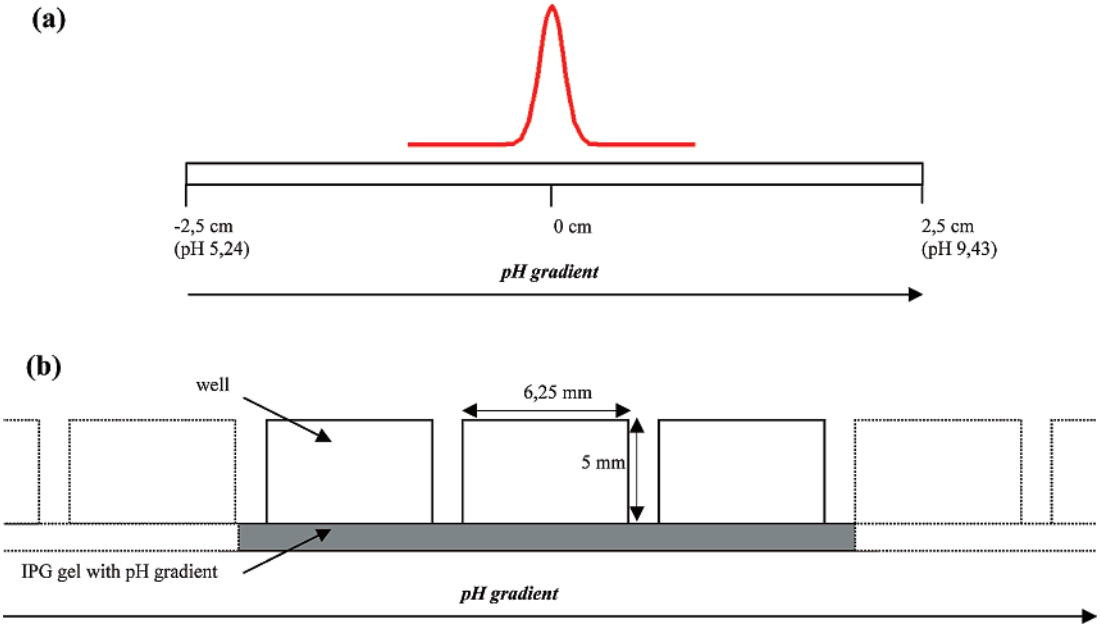

Figure 1. Geometries used in the simulation: (a) the 1-D geometry (calibration) is constituted of an IPG gel of 5 cm length; (b) the 2-D geometry is constituted of three or seven wells of 6.25 mm width, 5 mm height, and distant of 0.75 mm with an underlying IPG gel.

This differential equation describes the isoelectric focusing in a steady-state regime, the charge of the peptide being a function of the pH or of the distance (in the cases studied, the pH gradient is linear). Assuming a uniform electric field, eq 6 was solved analytically with Igor software (Wavemetrics, Portland) and allowed to display the steady-state concentration profile of the focused peptide for different values of electric field (no geometry effect taken into account here). This model will be taken as reference to validate the following Finite Element Model.

2.2. Finite Element Model. Numerous studies have been presented in the literature on the diffusion−migration phenomena to describe capillary electrophoresis or IEF processes.[36−42] Regarding OFFGEL, various finite element models based on diffusion, ampholyte reactions, and/or migration have been developed.[35,46,51] In the previous case of diffusion−migration-reaction of two model ampholytes,[46] one protonation site per ampholyte molecule was considered to facilitate the study. The main difference here is the consideration of not only one protonation site, but the global charge of the peptide, taking into account the many possible ionization sites existing on such a molecule, resulting in a pH-dependent global charge (as the pH is a function of the distance on the gel, the charge thus depends on the location of the peptide on the gel).

The numerical model was developed for 1-D and 2-D geometries and computes the peptides concentration profiles at different time steps of the focusing. The electric field was first calculated by solving the Laplace equation (eq 7).

$$\mathrm{div}(j) = \nabla(-\sigma\nabla\phi) = 0 \tag{7}$$

where j is the electrical current density and σ is the electrical conductivity. Next, the electric field $\nabla\phi$ was injected into eq 8, describing the transient transport of a species i by diffusion−migration

$$\frac{\partial c_i}{\partial t} + \nabla\left(-D_i\nabla c_i - \frac{z_i(\mathrm{pH}(x))F}{RT} D_i c_i \nabla\phi\right) = 0 \tag{8}$$

1-D geometry consists of a vertical cross-section of an IPG gel (Figure 1a) to study the influence of peptide charge gradient on the focusing time and focused peak width. 2-D geometry consists of a vertical cross-section of the multicompartment OFFGEL device (Figure 1b). The 2-D geometry (dimensions consistent with the experimental setup described by Michel et al.[18]) is used to study the influence of the well height and shape on the focusing, as well as to describe the IEF of three peptides under conditions close to experimental ones. The potential gradient applied across the gel as boundary conditions is 100 V·cm^{-1} for both 1-D and 2-D studies. The initial peptide concentration was fixed at 1 mM for all the calculations (uniform distribution along the gel and in the solution). The model was implemented on the finite element commercial software Flux-Expert (Astek Rhône-Alpes, Grenoble, France). More details on the numerical model, assumptions, and parameters are given in Supporting Information 2.

2.3. *In Silico* Proteome Digestion and Computation of Physicochemical Parameters. A program simulating tryptic digestion was written with Igor. Proteomes of *D. radiodurans*, *S. cerevisiae*, and *H. sapiens* were downloaded from the Swiss-Prot database through the Sequence Retrieval System (http://www.expasy.ch/ftp/) (July 2006). The homemade program was used to:

1. Perform the tryptic digestion of proteins with two miscleavages.

2. Calculate the MW and p*I* of peptides resulting from their sequence, using the amino acids p*K* values in Supporting Information 1[48].

3. Trace the titration curve for each peptides (net charge vs pH), and calculate the charge derivative at p*I*.

Values of p*I* were estimated by a secant algorithm from the titration curve, with a precision of 0.02 pH unit. The titration curve was obtained from the sequence of amino acids and based on eq 3. The charge slope d*z*/dpH at p*I* was obtained from the derivation in pH of eq 3. Peptide/protein masses and p*I* calculation were validated through manual comparison with **p*I*/MW compute** available on Expasy (http://www.expasy.ch).

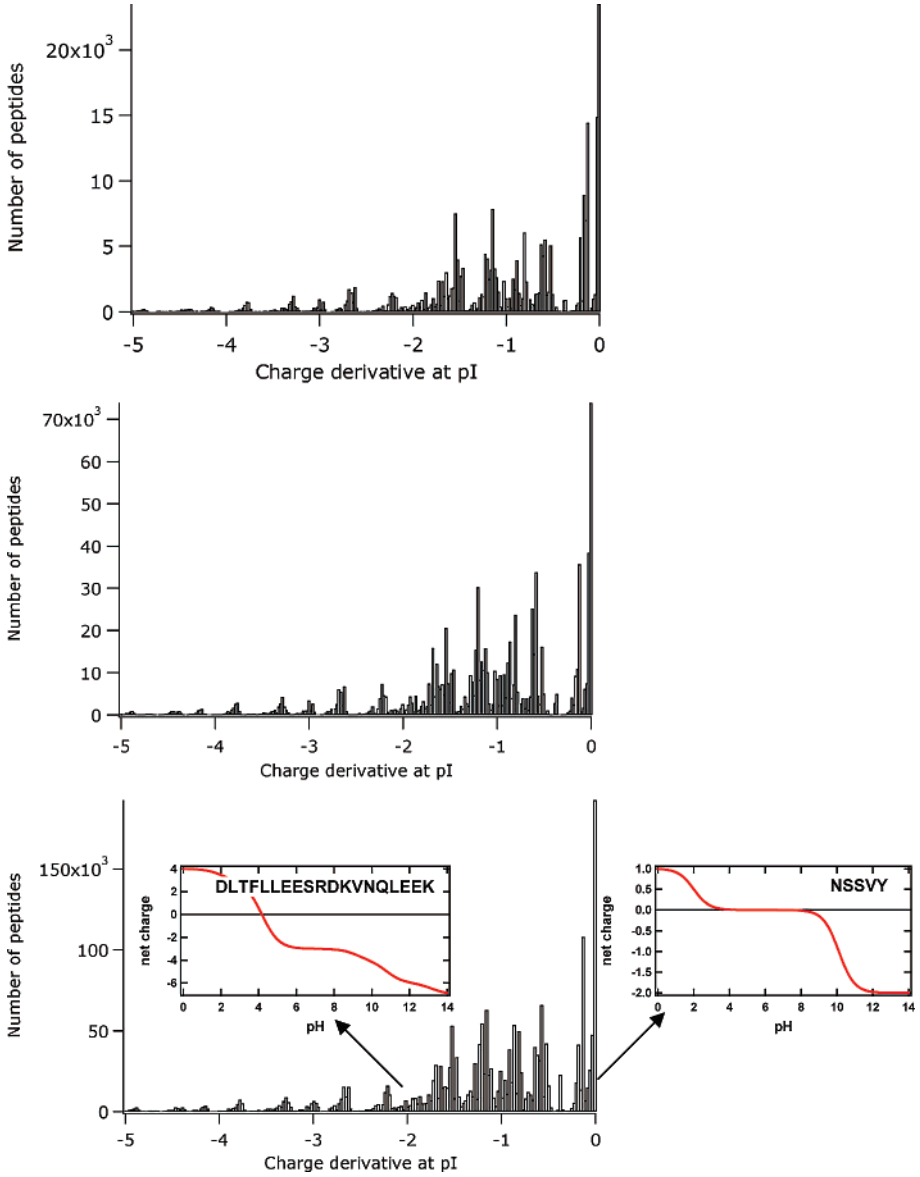

Figure 2. Distributions of charge derivative d*z*/dpH at p*I* for the peptides generated by the simulated digestion of *D. radiodurans* (top), *S. cerevisiae* (middle), and *H. sapiens* (bottom).

Values of p*I* are slightly different from those obtained with **p*I*/MW compute** due to the different values of pK_a used. The p*I* distribution of proteins was calculated for a few species and produced the well-known bimodal p*I* distribution[47] (data not shown), which adds to the validation of our calculations. The tryptic digestion was also validated by comparison to the tool MS-digest from http://prospector.ucsf.edu/.

Results and Discussion

3.1. Model Validation. The numerical model is validated by comparing the focused peaks obtained at steady state with the peaks calculated with the analytical model. The comparison shows a good agreement (Supporting Information 3). However, numerical simulations allow observing transient states of the focusing, whereas the analytical calculation gives results at the steady state of focusing only. Another drawback of the analytical model is the 1-D limitation. Following this validation, numerical simulations with Flux-Expert were used for further investigation.

3.2. Determination of the Order of Magnitude of d*z*/dpH at p*I*. The *in silico* tryptic digestion of the different proteomes was performed, and the resulting peptides were analyzed. Figure 2 shows the distribution of the charge derivative d*z*/dpH calculated at p*I* for peptides generated from the proteome digestion of *D. radiodurans*, *S. cerevisiae*, and *H. sapiens*. As shown, charge slopes are mostly comprised between 0 and −3. The highest bar corresponds to the "flattest" peptides, illustrated by the titration curve of the peptide NSSVY (see Figure 2, bottom). It is in that case more relevant to define a "p*I* zone" rather than a p*I* value, as the charge of the peptide does not vary much around its p*I*. The peptides having a charge derivative at p*I* comprised between −0.1 and −3 (illustrated by the titration curve peptide DLTFLLEESRDKVNQLEEK, Figure 2, bottom) represent 76.8% (*D. radiodurans*), 77.4% (*S. cerevisiae*), and 79.0% (*H. sapiens*). For these peptides, the charge gradient is steeper around the p*I*. Simply for comparison, as this study can be applied to proteins as well, the charge derivatives for proteins were calculated (results not shown) and

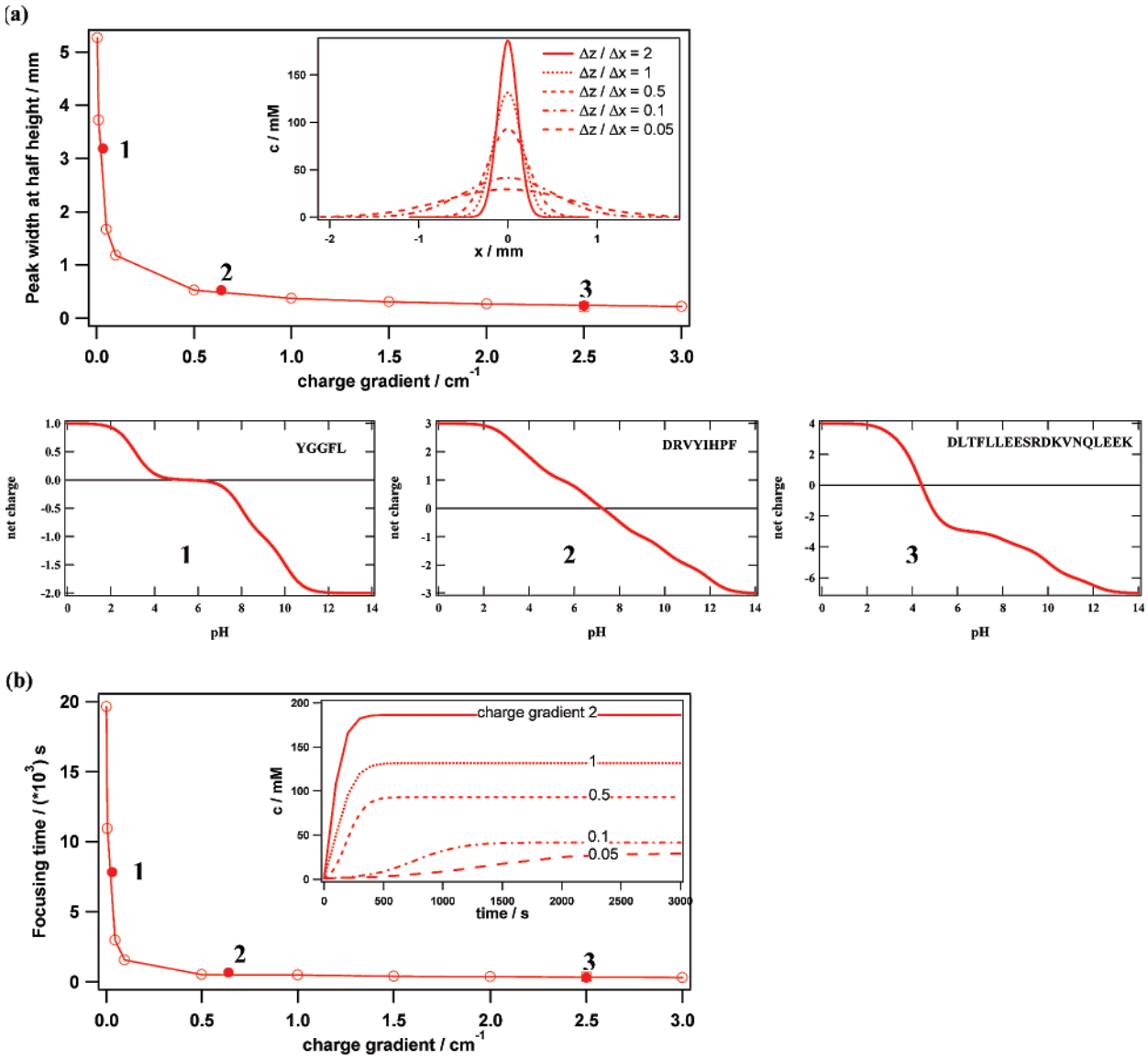

Figure 3. (a) Evolution of the focused peak width at half-height versus absolute values of charge gradient, (inset: focused peak for different linear charge gradients from 0.05 to 2 pH·cm^{-1}) and validation with three peptides: **(1)** leucine enkephalin (flat slope at p*I*), **(2)** angiotensin II (intermediate slope at p*I*), and **(3)** a peptide from the human proteome digestion (steep slope at p*I*). (b) Evolution of the focusing time versus charge gradient (inset: transient concentrations for different linear charge gradients from 0.05 to 2 pH·cm^{-1}).

unsurprisingly showed larger a range than that for peptides, as proteins' charge is higher than peptides' charge. For peptides, interestingly, the distribution of charge derivative is quite similar for the three organisms. It gives an overview of the diversity of peptides' charge properties near p*I* and allows estimating the range of charge slope at p*I*.

3.3. Effect of the Charge Gradient d*z*/d*x* at the p*I* (1-D Study). As seen in the previous distribution, the range of d*z*/dpH for most peptides from the digestion of different proteomes varies between − 0.1 and − 3. The charge gradient can be written as follows: (d*z*/d*x*) = (d*z*/dpH)(dpH/d*x*).

As the pH gradient dpH/d*x* is linear, if in a small region near the p*I* the slope of the titration curve d*z*/dpH is assumed to be linear, the charge gradient d*z*/d*x* will also be linear. In the following study, a value of 1 pH·cm^{-1} is taken for the pH gradient. The influence of a linear charge gradient value on the focusing will be studied numerically. The comparison with the case of peptides will be done to show that the peptide charge slope at p*I* is the key parameter for the focusing.

3.3.1. Effect on the Peak Width. Figure 3a shows the shape of the focused peak for different linear charge gradients from 0.05 to 2 (absolute values). As expected, the higher the charge gradient, the higher the final concentration and the narrower the focused peak width at steady state, because with a greater charge gradient, the mobility gradient is higher. The peak is thus more "focused" and concentrated. The effect of the charge slope at p*I* on the peak width was then studied for peptides, by giving as input to the simulation the expression of the charge as a function of pH. For this, three peptides were chosen according to their charge curve and slope at p*I*: leucine enkephalin (YGGFL), angiotensin II (DRVYIHPF), and a peptide from the human proteome digestion (DLTFLLEESRDKVNQLEEK) were used. Simulations of IEF were performed on these peptides, and the focused peak width at steady state was reported for each one on Figure 3a. The peptides fit to the curve deduced from linear charge gradients, which validates the idea that the slope near p*I* is the most important factor, and the

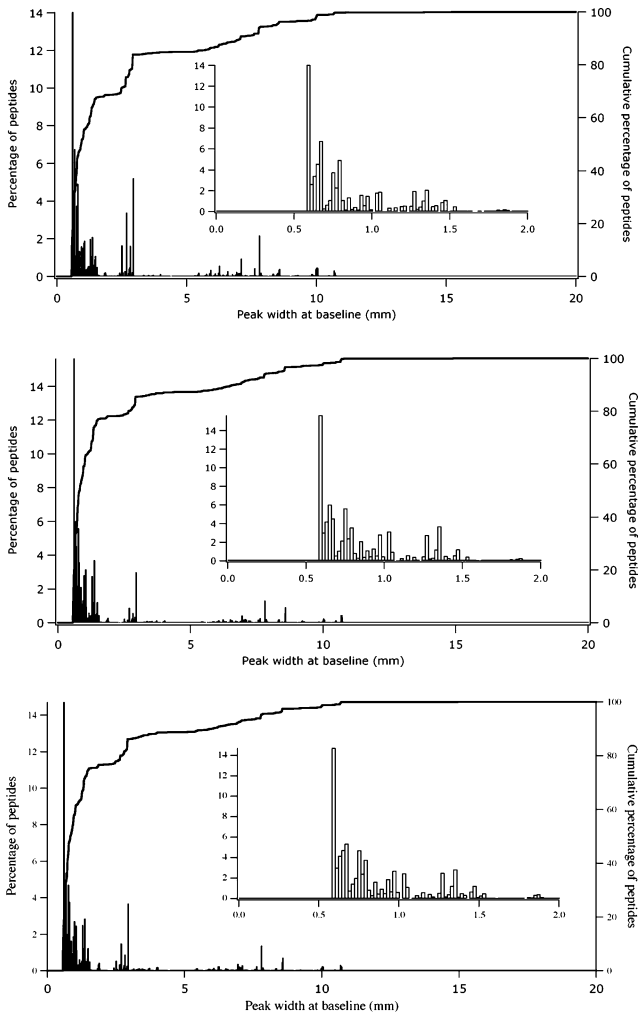

Figure 4. Histogram of peak widths at baseline, as fitted from the numerical simulations for *D. radiodurans* (top), *S. cerevisiae* (middle), and *H. sapiens* (bottom). In each graph, the inset shows a magnification of the bar histogram, and the continuous line shows the cumulative percentage of peptides focusing with a given peak width.

shape of the titration curve far from p*I* has no influence on the width of the focused peak.

From the top panel of Figure 3, the theoretical peak width of any peptide can be calculated from its charge derivative at p*I*. Figure 4 thus shows the theoretical peak width distributions of *in silico* digested proteomes; bars represent the percentage of peptides focusing with a given peak width at baseline, whereas the continuous line shows the percentage of peptides focusing with a peak width at baseline below a given value. Interestingly, the three species exhibit a very similar peak width distribution, which demonstrates the versatility of OFFGEL electrophoresis in the context of shotgun proteomics. Additionally, for the three species considered, around 90% of peptides focus within less than 6 mm (the well width used in practice), which means that in theory, 90% of peptides should be recovered in no more than two wells. This result is well in line with the experimental findings of Hörth et al. who found that 74% of tryptic peptides of *E. coli* focus in one well, and 90% focus in two wells at most.[32]

3.3.2. Effect on the Focusing Time. Figure 3b illustrates the evolution of the focusing time for different values of linear charge gradient from 0.05 to 2 (absolute values). The steeper the charge gradient at p*I*, the higher the final concentration and the faster the steady state is reached. As previously stated, to validate our approach (linearization of the charge slope at p*I*), the effect of peptide charge slope at p*I* on the focusing time was studied. For this, the same peptides as before were used. For each of them, the focusing time (defined as the time needed to reach 99% of the steady-state concentration) was reported on Figure 3b. For the three peptides, focusing times fit to the linear gradient curve, showing that the slope at p*I* is the key parameter for the focusing time as well. As a consequence, the shape of the titration curve far from p*I* has no influence on the focusing time. One can easily understand this tendency by seeing that the migration velocity far from p*I* is so high that only the migration near p*I* determines the kinetics of focusing, as the limiting factor.

In this section, it was shown that, given the distribution of dz/dpH for the *in silico* digested proteomes (charge gradient between −0.1 and −3), and if taking a particular pH gradient (e.g., pH 3−10 on a 13 cm long strip), an optimal dimension of the well can be given, for a chosen percentage of correctly focused peptides. It is estimated that the optimal well width in an OFFGEL device (given by the largest peak width obtained with a flat titration curve) is 6−7 mm, which allows recovering 90% of peptides in at most two wells.

From the main results on the peak width and focusing time, some practical conclusions can be drawn for the IEF of peptides in an OFFGEL device. Assuming the initial peptide sample solution is loaded in all the wells, the starting voltage should be low in the first step. As we see, the focusing process is quite fast at the start, as most of the species are highly charged (far from p*I*). In practice, the presence of salts accompanying the sample at the start should be taken into account as well. Thus, a low starting voltage should allow performing efficient focusing meanwhile avoiding too much heating. Then the voltage should be increased gradually or stepwise to reach the steady state of focusing, as the charge decreases, and the closer the species gets to its p*I*, the slower it is migrating. Thus, to allow a sharp focusing at the end, it is recommended to apply a high final voltage. The current, if monitored, is also a good indicator of the advancement of the focusing process. The current at the beginning is at the maximum (highly charged species migrating) and should decrease to finally reach a steady-state residual value (dynamic equilibrium between migration and diffusion). To give an idea of the focusing time, some authors have recently published interesting results concerning the IEF of peptides in gel,[23] and papers concerning the OFFGEL IEF of peptides can be taken as reference.[30,32,33]

Concerning the use of peptides' p*I* as a filtering/validating tool in the identification of peptides and proteins, not only the p*I* value is important, but also the slope of the titration curve at p*I*. Thus, in setting the limits of exclusion based on the p*I* of peptides, this slope should also be taken into account, to avoid eliminating true peptides, which did focus but in several wells, due to their characteristic titration curve.

3.4. Effect of the Well Height on the Recovery and Focusing Time (2-D Study). To study the influence of the well height on the focusing, numerical simulation of OFFGEL IEF was performed for a given peptide (Angiotensin II) in a three-compartment device. Different height ratios were studied: $h_{well}/h_{gel} = 1$, 2, 4, and 10. Figure 5 displays the peptide concentration at different time steps, for the ratios $h_{well}/h_{gel} = 10$ (high wells)

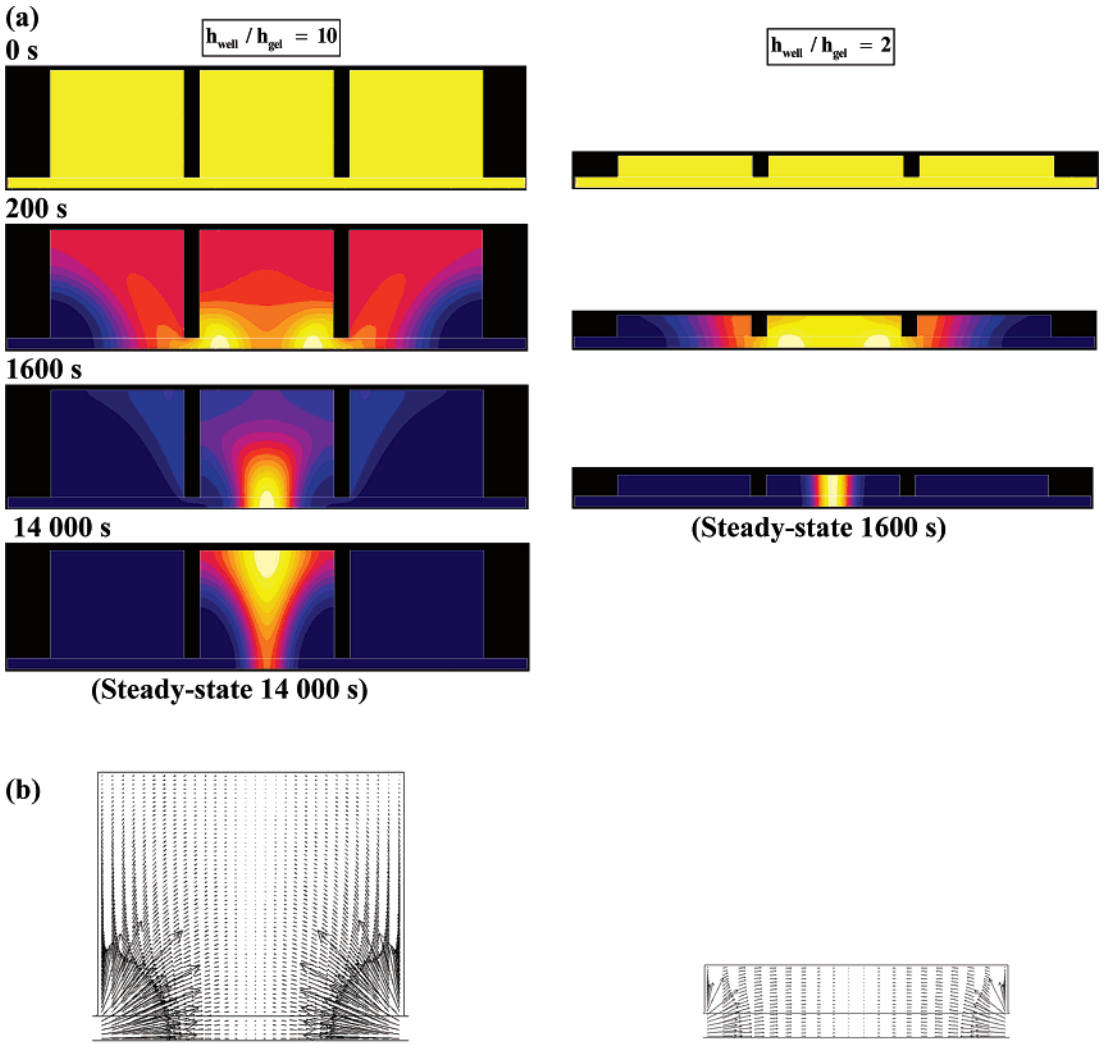

Figure 5. Effect of the well height: (a) concentration isovalues of angiotensin II (p*I* = 7.25) at different times for two height ratios h_{well}/h_{gel} = 10 and 2. IEF conditions: constant applied voltage of 100 V·cm^{-1} and pH gradient of 0.5 pH·cm^{-1}. (b) Distribution of the current lines in the wells under the same conditions.

and h_{well}/h_{gel} = 2 (low wells). The initial concentration of peptides was fixed at 1 mM for all the calculations.

The focusing can be described in two phases. These two phases can be best seen for h_{well}/h_{gel} = 10 on Figure 5a. In a first phase (for times <800 s), the peptide migrates essentially in the gel underneath the wells toward its p*I* (***horizontal focusing***). In a second phase (for times >800 s), the species diffuses to the solution in the well (***vertical focusing*** due to 2-D geometry). For the low wells, h_{well}/h_{gel} = 2 , the process consists mostly of the first phase, because the vertical focusing is strongly limited by the height of the well. The two focusing steps can be correlated with the distribution of migration velocities, shown in Figure 5b for both height ratios. In a high well, the migration velocity has a non-negligible vertical component, which is the driving force for the vertical focusing, whereas in the low well, the current lines are all parallel to the gel (except at the corners). The vertical focusing is quasi nonexistent. Thus, it takes approximately 10 times longer to reach the steady state in high wells than it does in low wells (14 000 s for a height ratio of 10 vs 1600 s for a height ratio of 2). In the high well, once the species reaches the top of the well, the solution horizontal focusing gives broader shape, due to the lower local values of the migration (i.e., electric field) compared to the diffusion.

However, the final to initial quantity ratio recovered in solution is higher for the high wells, as shown in Figure 6. The recovery percentage is an interesting parameter, which is defined as the ratio of the quantity of focused species in the central well to the initial quantity (i.e., in all the wells and the gel) and noted n_{well}/n_{tot}. It illustrates that although the steady state is reached faster for low wells than for high wells, the recovery is still better for high wells. For height ratios of h_{well}/h_{gel} = 10, 4, and 1, recovery of 96%, 82%, and 50% were obtained, respectively. These values of recovery could be theoretically predicted by geometrical considerations, as shown in Figure 6, where the values theoretically expected for the recovery are 91%, 80%, and 50%, respectively, for height ratios of 10, 4, and 1. The 2-D effect of the vertical focusing is amplifying the recovery for high wells (5% more than the predicted recovery for height ratio of 10). This enhancement in the recovery observed for high wells can be explained by the higher proportion of current lines penetrating the well compared to the ones in the gel (Figure 5b).

3.5. Effect of the Well Shape on the Recovery and Focusing Time. The effect of the well shape was also studied. In

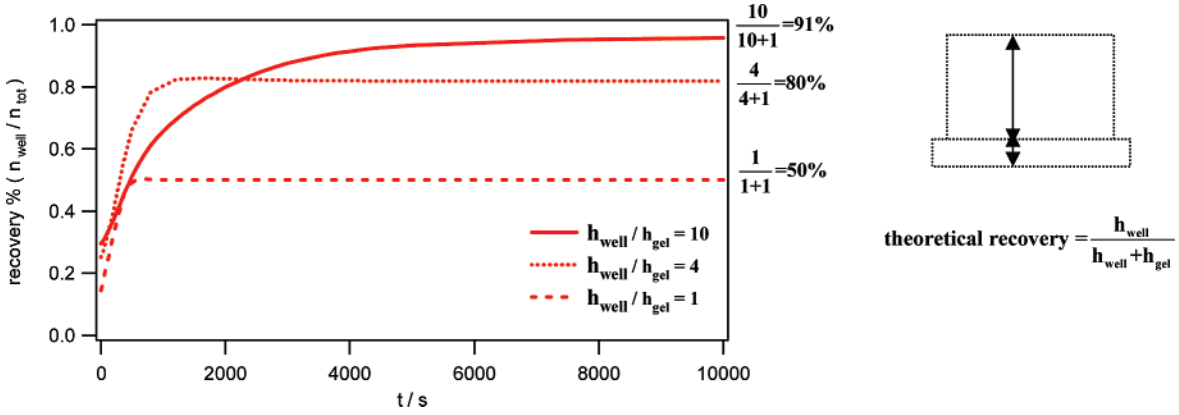

Figure 6. Recovery percentage in the focusing well solution versus time for different height ratios h_{well}/h_{gel}.

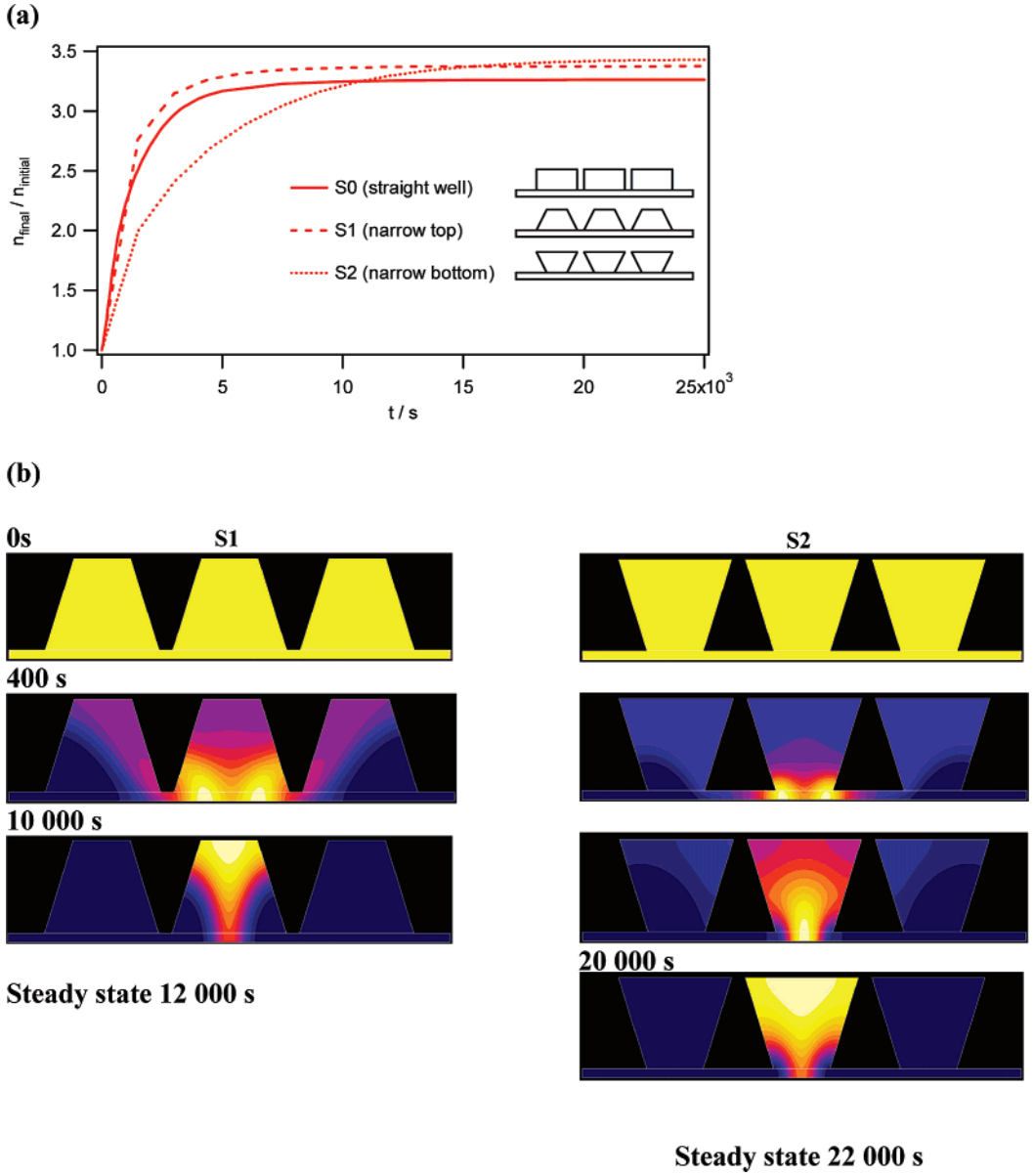

Figure 7. (a) Final to initial peptide concentration ratio in the focusing well (mean value), for three different well shapes. (b) Peptide concentration isovalues for narrow-top and narrow-bottom wells at different time steps. Same IEF conditions as in Figure 5.

particular, three shapes were considered, as illustrated in Figure 7, and compared to determine which shape should be optimal for the IEF. Shape S0 is the straight well used for the simulations presented above. S1 is the well with narrow top, and S2 is the well with narrow bottom. The concentration factor, defined as the ratio of final concentration to initial concentration in the

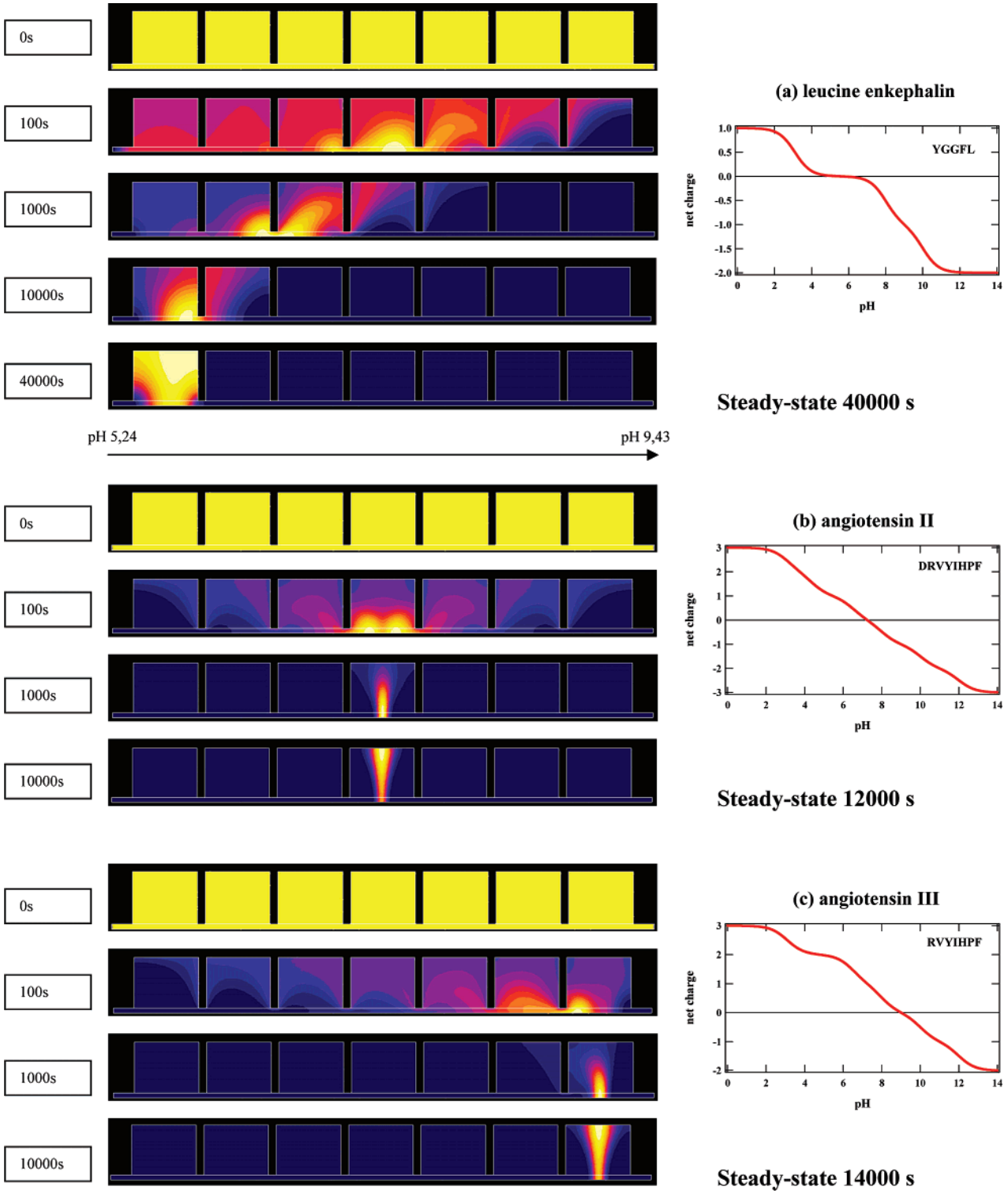

Figure 8. Peptide concentration isovalues in a seven-compartment OFFGEL device. IEF conditions: all initial concentrations 1 mM, pH gradient = 0.8 pH unit·cm^{-1}, voltage = 100V·cm^{-1}.

focusing well solution, is displayed in Figure 7a for different shapes. The concentration factor is slightly higher for the shapes S1 and S2, compared with S0 (straight well), which indicates that the recovery should be only slightly higher for these shapes, if the initial concentration is the same in all cases. But most striking is the difference in focusing time. For narrow-top and straight wells, the focusing is almost 2 times faster than for narrow-bottom wells (12 000 and 14 000 s versus 22 000 s, respectively). This difference in focusing times could be explained by the presence of "dead zones" in S2 (see Figure 7b). These are the zones in the top corners of the well, where the electric current lines are quasi nonexistent. Consequently, the migration in these zones is not efficient, and only diffusion takes place. In S1, where these zones are reduced because of the narrow top, the steady state is reached faster than in S2. Moreover, in S2, the current lines have to go through a longer

way to enter the basis of wells (see Figure 7b), thus, adding to the time needed to reach steady state. However, in terms of practicability, the straight wells or wide-top wells should be better to introduce or retrieve the sample.

3.6. IEF of Peptides in a Seven-Well Device. Three peptides (leucine enkephalin, angiotensin II, and angiotensin III) were used to visualize the focusing in an OFFGEL device with seven wells. IEF conditions were as close as possible to the experimental conditions. A constant voltage was applied between anode and cathode (mean value of 100 $V \cdot cm^{-1}$); a pH gradient of 0.8 $pH \cdot cm^{-1}$ was taken (for comparison, a 3−10 pH gradient on a 13 cm strip for OFFGEL IEF gives a pH gradient of 0.54 $pH \cdot cm^{-1}$). Figure 8 displays the concentration isovalues for each peptide at different time steps. Here as well, the two phases of horizontal and vertical focusing are observed, especially clearly for the "flat peptide". At 100 s, that peptide is still migrating toward the well corresponding to its p*I*, whereas the other two peptides, which are steeper, have already reached their focusing well. For comparison, the ratio of focusing time for the flat peptide over the one for steep peptide (t_{flat}/t_{steep}) is 3.33 for 2-D geometry, while it was equal to 8.89 for 1-D geometry. This shows clearly the 2-D effect, which tends to reduce the discrepancy between a flat and a steep peptide in terms of focusing time. This could be explained by the vertical focusing step, during which the steep peptide is "losing its advance" on the "flat peptide". Not much difference was observed between the focusing times of the last two peptides, and their charge slope at p*I* was very close (0.64 for angiotensin II and 0.49 for angiotensin III). Even though the distance to migrate is longer for angiotensin III than for angiotensin II, only the charge slope at p*I* is to be considered, and for this case, it does not induce a big difference in focusing time.

4. Concluding Remarks

A preliminary *in silico* tryptic digestion of the proteomes from three different organisms was performed, to give an overview of the distribution of peptide charge slopes at p*I*. The influence of this charge slope at p*I* was then investigated. The main result is that this slope not only acts on the focused peak shape, but also constitutes the limiting factor in the focusing kinetics, the charge far from p*I* having no influence. By modeling the peak width as a function of the charge gradient at p*I*, we demonstrated that 90% of peptides should be correctly focused in at most two wells, considering the geometry used. This interestingly confirms recent experimental results and strongly suggests the high-resolution power of OFFGEL and its relevance in shotgun proteomic strategies. Concerning the use of peptides' p*I* as a filtering/validating tool in the identification of peptides and proteins, not only the p*I* value, but also the slope of the titration curve at p*I* are important when setting the limits of exclusion based on the p*I* of peptides. Other geometrical parameters were also investigated (well height and shape). For higher wells, the recovery of peptides is much more important than for lower wells, although it takes longer to recover the maximal quantity of peptides. As for the shape of the wells, straight or narrow-top wells are optimal for faster focusing.

Acknowledgment. The authors wish to acknowledge the Swiss National Science Foundation for financial support (Grant number 200020-105489).

Supporting Information Available: Supporting Information 1 is the table of pK_a values used for the calculations. Supporting Information 2 gives details about assumptions and parameters of the simulation (Peclet number, mesh size, and integral Galerkin formulation for the simulation equations). Supporting Information 3 is a figure showing the validation of the numerical model, based on the comparison with the analytical calculations. This material is available free of charge via the Internet at http://pubs.acs.org.

References

(1) Rabilloud, T.; Luche, S.; Chevallet, M. *Biofutur* **2002**, 11−19.
(2) Gorg, A.; Weiss, W.; Dunn, M. J. *Proteomics* **2004**, *4*, 3665−3685.
(3) Rabilloud, T. *Proteomics* **2002**, *2*, 3−10.
(4) Domon, B.; Aebersold, R. *Science* **2006**, *312*, 212−217.
(5) Righetti, P. G.; Castagna, A.; Antonioli, P.; Boschetti, E. *Electrophoresis* **2005**, *26*, 297−319.
(6) Righetti, P. G.; Castagna, A.; Herbert, B.; Reymond, F.; Rossier, J. S. *Proteomics* **2003**, *3*, 1397−1407.
(7) Hoffmann, P.; Ji, H.; Moritz, R. L.; Connolly, L. M.; Frecklington, D. F.; Layton, M. J.; Eddes, J. S.; Simpson, R. J. *Proteomics* **2001**, *1*, 807−818.
(8) Zischka, H.; Weber, G.; Weber, P. J. A.; Posch, A.; Braun, R. J.; Buhringer, D.; Schneider, U.; Nissum, M.; Meitinger, T.; Ueffing, M.; Eckerskorn, C. *Proteomics* **2003**, *3*, 906−916.
(9) Moritz, R. L.; Ji, H.; Schutz, F.; Connolly, L. M.; Kapp, E. A.; Speed, T. P.; Simpson, R. J. *Anal. Chem.* **2004**, *76*, 4811−4824.
(10) Weber, G.; Islinger, M.; Weber, P.; Eckerskorn, C.; Volkl, A. *Electrophoresis* **2004**, *25*, 1735−1747.
(11) Moritz, R. L.; Simpson, R. J. *Nat. Methods* **2005**, *2*, 863−873.
(12) Moritz, R. L.; Skandarajah, A. R.; Ji, H.; Simpson, R. J. *Comp. Funct. Genomics* **2005**, *6*, 236−243.
(13) Righetti, P. G.; Wenisch, E.; Faupel, M. *J. Chromatogr.* **1989**, *475*, 293−309.
(14) Herbert, B.; Righetti, P. G. *Electrophoresis* **2000**, *21*, 3639−3648.
(15) Pedersen, S. K.; Harry, J. L.; Sebastian, L.; Baker, J.; Traini, M. D.; McCarthy, J. T.; Manoharan, A.; Wilkins, M. R.; Gooley, A. A.; Righetti, P. G.; Packer, N. H.; Williams, K. L.; Herbert, B. R. *J. Proteome Res.* **2003**, *2*, 303−311.
(16) Wall, D. B.; Kachman, M. T.; Gong, S. Y.; Hinderer, R.; Parus, S.; Misek, D. E.; Hanash, S. M.; Lubman, D. M. *Anal. Chem.* **2000**, *72*, 1099−1111.
(17) Ros, A.; Faupel, M.; Mees, H.; van Oostrum, J.; Ferrigno, R.; Reymond, F.; Michel, P.; Rossier, J. S.; Girault, H. H. *Proteomics* **2002**, *2*, 151−156.
(18) Michel, P. E.; Reymond, F.; Arnaud, I. L.; Josserand, J.; Girault, H. H.; Rossier, J. S. *Electrophoresis* **2003**, *24*, 3−11.
(19) Essader, A. S.; Cargile, B. J.; Bundy, J. L.; Stephenson, J. L. *Proteomics* **2005**, *5*, 24−34.
(20) Cargile, B. J.; Talley, D. L.; Stephenson, J. L. *Electrophoresis* **2004**, *25*, 936−945.
(21) Cargile, B. J.; Bundy, J. L.; Freeman, T. W.; Stephenson, J. L. *J. Proteome Res.* **2004**, *3*, 112−119.
(22) Cargile, B. J.; Stephenson, J. L. *Anal. Chem.* **2004**, *76*, 267−275.
(23) Krijgsveld, J.; Gauci, S.; Dormeyer, W.; Heck, A. J. R. *J. Proteome Res.* **2006**, *5*, 1721−1730.
(24) Xie, H.; Rhodus, N. L.; Griffin, R. J.; Carlis, J. V.; Griffin, T. J. *Mol. Cell. Proteomics* **2005**, *4*, 1826−1830.
(25) Xie, H.; Bandhakavi, S.; Griffin, T. J. *Anal. Chem.* **2005**, *77*, 3198−3207.
(26) Xie, H. W.; Bandhakavi, S.; Griffin, T. J. *Anal. Chem.* **2005**, *77*, 3198−3207.
(27) Tan, A. M.; Pashkova, A.; Zang, L.; Foret, F.; Karger, B. L. *Electrophoresis* **2002**, *23*, 3599−3607.
(28) Baczek, T. *J. Pharm. Biomed. Anal.* **2004**, *35*, 895−904.
(29) Baczek, T. *J. Pharm. Biomed. Anal.* **2004**, *34*, 851−860.
(30) Heller, M.; Michel, P. E.; Morier, P.; Crettaz, D.; Wenz, C.; Tissot, J. D.; Reymond, F.; Rossier, J. S. *Electrophoresis* **2005**, *26*, 1174−1188.
(31) Heller, M.; Ye, M. L.; Michel, P. E.; Morier, P.; Stalder, D.; Junger, M. A.; Aebersold, R.; Reymond, F. R.; Rossier, J. S. *J. Proteome Res.* **2005**, *4*, 2273−2282.
(32) Hörth, P.; Miller, C. A.; Preckel, T.; Wenz, C. *Mol. Cell. Proteomics* **2006**, *5*, 1968−1974.
(33) Michel, P. E.; Crettaz, D.; Morier, P.; Heller, M.; Gallot, D.; Tissot, J. D.; Reymond, F.; Rossier, J. S. *Electrophoresis* **2006**, *27*, 1169−1181.
(34) Burgess, J. A.; Lescuyer, P.; Hainard, A.; Burkhard, P. R.; Turck, N.; Michel, P.; Rossier, J. S.; Reymond, F.; Hochstrasser, D. F.; Sanchez, J. C. *J. Proteome Res.* **2006**, *5*, 1674−1681.

(35) Arnaud, I. L.; Josserand, J.; Rossier, J. S.; Girault, H. H. *Electrophoresis* **2002**, *23*, 3253−3261.
(36) Thormann, W.; Mosher, R. A.; Bier, M. *J. Chromatogr.* **1986**, *351*, 17−29.
(37) Mosher, R. A.; Thormann, W.; Bier, M. *J. Chromatogr.* **1988**, *436*, 191−204.
(38) Mosher, R. A.; Dewey, D.; Thormann, W.; Saville, D. A.; Bier, M. *Anal. Chem.* **1989**, *61*, 362−366.
(39) Mosher, R. A.; Thormann, W. *Electrophoresis* **1990**, *11*, 717−723.
(40) Mosher, R. A.; Thormann, W. *Electrophoresis* **2002**, *23*, 1803−1814.
(41) Thormann, W.; Huang, T. M.; Pawliszyn, J.; Mosher, R. A. *Electrophoresis* **2004**, *25*, 324−337.
(42) Thormann, W.; Mosher, R. A. *Electrophoresis* **2006**, *27*, 968−983.
(43) Mosher, R. A.; Bier, M.; Righetti, P. G. *Electrophoresis* **1986**, *7*, 59−66.
(44) Tonani, C.; Faupel, M.; Righetti, P. G. *Electrophoresis* **1991**, *12*, 631−636.
(45) Tonani, C.; Righetti, P. G. *Electrophoresis* **1991**, *12*, 1011−1021.
(46) Di Maio, I. Ph.D. Thesis (Thesis No 3064), Ecole Polytechnique Fédérale de Lausanne, Switzerland, 2004.
(47) Weiller, G. F.; Caraux, G.; Sylvester, N. *Proteomics* **2004**, *4*, 943−949.
(48) *CRC Handbook of Chemistry and Physics*, 87th ed.; CRC Press: Boca Raton, FL, 2006−2007.
(49) Bjellqvist, B.; Hughes, G. J.; Pasquali, C.; Paquet, N.; Ravier, F.; Sanchez, J. C.; Frutiger, S.; Hochstrasser, D. *Electrophoresis* **1993**, *14*, 1023−1031.
(50) Halligan, B. D.; Ruotti, V.; Jin, W.; Laffoon, S.; Twigger, S. N.; Dratz, E. A. *Nucleic Acids Res.* **2004**, *32*.
(51) Arnaud, I. L.; Josserand, J.; Jensen, H.; Lion, N.; Roussel, C.; Girault, H. H. *Electrophoresis* **2005**, *26*, 1650−1658.

PR0606023